Original Article

A physiological study to determine the mechanism of carbon dioxide clearance during apnoea when using transnasal humidified rapid insufflation ventilatory exchange (THRIVE)*

L. A. Hermez,[1] **C. J. Spence,**[1] **M. J. Payton,**[2] **S. A. R. Nouraei,**[4] **A. Patel**[5] and **T. H. Barnes**[3,6,7]

1 Senior Research Scientist, 2 General Manager, 3 Consultant, Anaesthesia Research Group, Fisher and Paykel Healthcare Ltd, Auckland, New Zealand
4 Consultant Laryngologist, Robert White Centre for Airway Voice and Swallowing, Poole Hospital NHS Foundation Trust, Poole, UK
5 Consultant Anaesthetist, Department of Anaesthesia, Royal National Throat, Nose and Ear Hospital in UCLH, London, UK
6 Director, Science and Technology Solutions Ltd, Warlingham, UK
7 Emeritus Professor, University of Greenwich, London, UK

Summary

Clinical observations suggest that compared with standard apnoeic oxygenation, transnasal humidified rapid-insufflation ventilatory exchange using high-flow nasal oxygenation reduces the rate of carbon dioxide accumulation in patients who are anaesthetised and apnoeic. This suggests that active gas exchange takes place, but the mechanisms by which it may occur have not been described. We used three laboratory airway models to investigate mechanisms of carbon dioxide clearance in apnoeic patients. We determined flow patterns using particle image velocimetry in a two-dimensional model using particle-seeded fluorescent solution; visualised gas clearance in a three-dimensional printed trachea model in air; and measured intra-tracheal turbulence levels and carbon dioxide clearance rates using a three-dimensional printed model in air mounted on a lung simulator. Cardiogenic oscillations were simulated in all experiments. The visualisation experiments indicated that gaseous mixing was occurring in the trachea. With no cardiogenic oscillations applied, mean (SD) carbon dioxide clearance increased from 0.29 (0.04) ml.min^{-1} to 1.34 (0.14) ml.min^{-1} as the transnasal humidified rapid-insufflation ventilatory exchange flow rate was increased from 20 l.min^{-1} to 70 l.min^{-1} (p = 0.0001). With a cardiogenic oscillation of 20 ml.beat^{-1} applied, carbon dioxide clearance increased from 11.9 (0.50) ml.min^{-1} to 17.4 (1.2) ml.min^{-1} as the transnasal humidified rapid-insufflation ventilatory exchange flow rate was increased from 20 l.min^{-1} to 70 l.min^{-1} (p = 0.0014). These findings suggest that enhanced carbon dioxide clearance observed under apnoeic conditions with transnasal humidified rapid-insufflation ventilatory exchange, as compared with classical apnoeic oxygenation, may be explained by an interaction between entrained and highly turbulent supraglottic flow vortices created by high-flow nasal oxygen and cardiogenic oscillations.

....

Introduction

High-flow nasal oxygenation entails administration of warmed and humidified oxygen-enriched air at flow rates between 40 l.min^{-1} and 60 l.min^{-1} to patients who are breathing spontaneously via a special purpose nasal cannula [1–4]. High-flow nasal oxygenation is effective in the intensive care setting for treating hypoxaemia [5], reducing reintubation rates [6] and has been shown to reduce 90-day mortality in this patient group [7].

Patel and Nouraei coined the term transnasal humidified rapid-insufflation ventilatory exchange (THRIVE) [8]; they delivered 100% oxygen at 70 l.min^{-1} using the Optiflow THRIVE^{TM} apparatus (Fisher and Paykel Healthcare Ltd, Auckland, New Zealand) to adult patients with known or anticipated difficult airways having general anaesthesia, with the aim of increasing safe apnoea time during intubation attempts. They observed not only an extension of time until desaturation, but also a significantly lower rate of carbon dioxide accumulation than would have been expected with 'classical' apnoeic oxygenation [8–11]. Further studies have also shown reduced accumulation of carbon dioxide [12–14].

The underlying mechanisms by which gas exchange may be taking place during high-flow nasal oxygenation under apnoeic conditions have not been elucidated. These are critical to understanding the efficacy and limitations of the technique, especially over extended apnoeic periods when hypercapnoea might become problematic.

In the early 1980s, Slutsky proposed that cardiogenic oscillations could be a major contributor to apnoeic oxygenation and gas exchange [15, 16]. Cardiogenic oscillations refer to changes in airway gas flow and pressure that are synchronous with the cardiac cycle [17, 18], and are believed to arise from the movement of blood in pulmonary vessels, causing compression and expansion of the small airways [19]. As under apnoeic conditions the principal intrinsic gas flow within the airway relates to cardiogenic oscillations, we hypothesised that an interaction between supraglottic turbulence generated by high-flow nasal oxygenation and cardiogenic oscillations might be contributing to the underlying mechanism of THRIVE.

The objective of this study was to examine the fluid dynamics affecting carbon dioxide clearance from the carina to the mouth in THRIVE, and calculate the likely rates of carbon dioxide clearance. We investigated fluid flow patterns using in-vitro laboratory models, and used the same models in conjunction with a specialised lung simulator to measure carbon dioxide clearance.

Methods

We used two 1:1 scale physical airway models obtained from clinical computerised tomography scans, that had previously been used as part of experiments to determine flow patterns and carbon dioxide distributions in spontaneous breathing with the application of high-flow nasal oxygenation (Fig. 1) [20]. These models were used to visualise supraglottic flow patterns and gas flow from the bronchi to the mouth; measure upper airway turbulence; and measure carbon dioxide clearance.

In all experiments, we used cardiogenic stroke volumes of 0–40 ml, with a cardiogenic oscillation flow profile shown by Tusman et al. [19]. Throughout our experiments, we defined an upwards flow in the airway, caused by cardiac systole, as cardiogenic expiration and downwards flow in the airway, which occurs during cardiac diastole, as cardiogenic inspiration.

For the visualisation of a supraglottic flow pattern, we used a transparent, two-dimensional airway model that had a 10-mm-thick rectangular cross-section (Fig. 1a). The shape corresponded to the mean midsagittal section of the CT airway scan. The working fluid was water that was seeded with neutrally buoyant tracer particles pumped into the nares and out of the mouth at a constant flow rate. Particle image velocimetry (PIVview2C; PIVtech, Gottingen, Germany) was used to determine the flow patterns. Cardiogenic oscillations were simulated by an oscillating syringe pump in the lung compartment. The oscillations were scaled to the value we estimated for cardiogenic oscillations in air at 70 beats.min^{-1}, using accepted flow model matching techniques [21, 22].

For visualisation of gas flow and carbon dioxide clearance from the bronchi to the mouth, we used a transparent three-dimensional printed version of the airway model described above, including the carina to the fifth generation (Fig. 1b). A cannula placed within the nares of the model provided nasal flow at rates of up to 70 l.min^{-1}. A nebuliser (Aerogen, Galway, Ireland) continuously filled the carina of the model with 1.5–3-µm-diameter water droplets. A video camera recorded flow and density patterns of nebulised gas in the trachea. A cardiogenic stroke volume of 20 ml at a heart rate of 70 beats.min^{-1} was simulated. This was achieved by the bronchioles protruding into a sealed plenum that was connected to a syringe pump.

For turbulence intensity and carbon dioxide clearance measurements (Fig. 1c), the three-dimensional printed airway model described above, extending to the distal end of the trachea, was mounted on top of a cylindrical plenum.
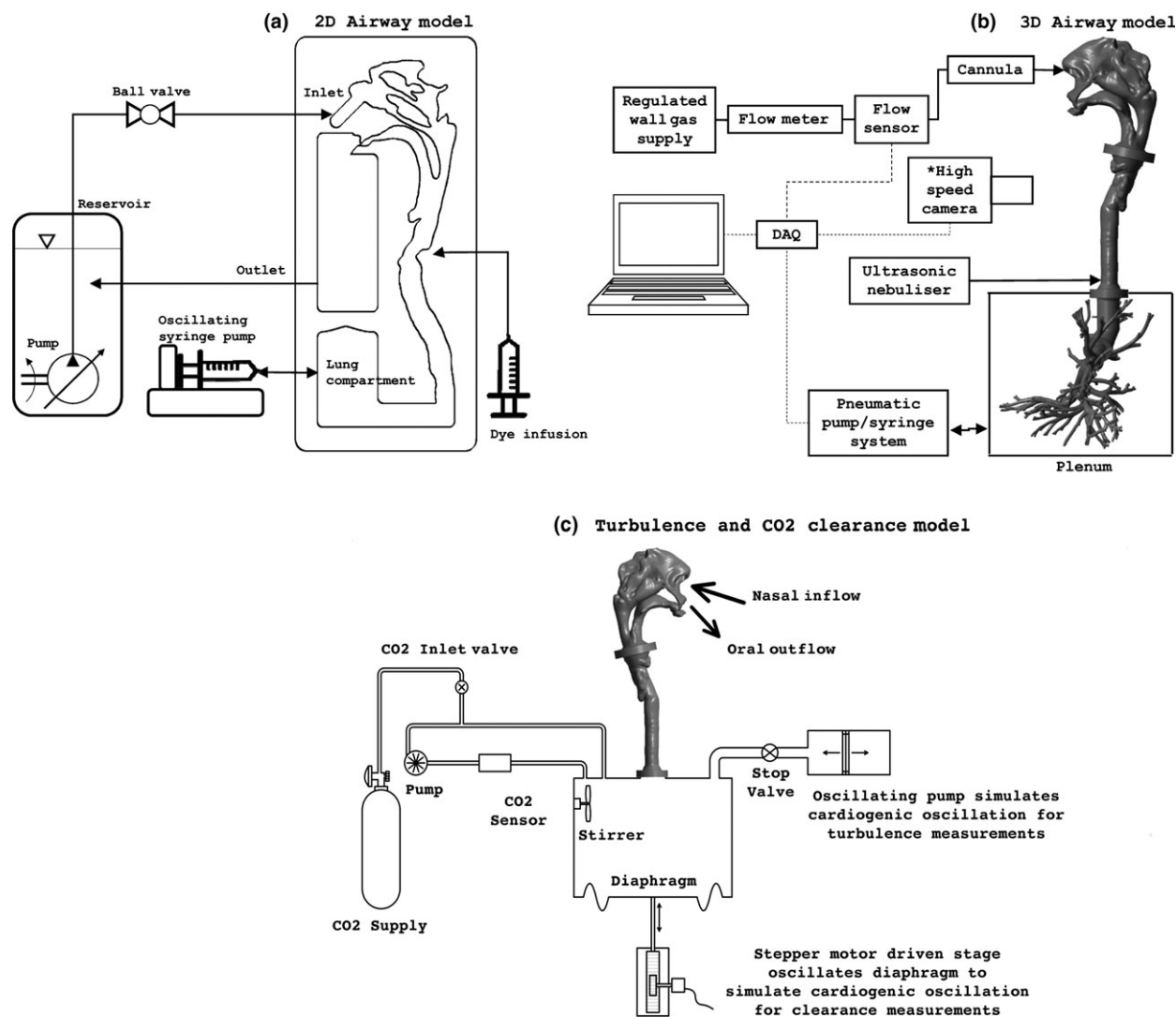
Figure 1 Schematics of the three models used for the experiments: (a) two-dimensional fluid model used for flow visualisation with particle image velocimetry; (b) three-dimensional gas model used to visualise transport of gas between carina and mouth; and (c) three-dimensional model and lung simulator used for turbulence and carbon dioxide clearance measurements. DAQ, data acquisition system.

Turbulence in the model was measured using a hot wire anemometer (HWA1; Science and Technology Solutions Ltd, Warlingham, UK). The model trachea was modified for these measurements with three ports, allowing insertion of the hot wire probe into the airway. The ports were located 1 cm below the glottis at the subglottis, at the mid-trachea, and 2 cm above the carina. Turbulence intensity was measured separately over the inspiration and expiration phases of several cardiogenic cycles, for THRIVE flows of 1 l.min^{-1}, 35 l.min^{-1} and 70 l.min^{-1} at a cardiogenic stroke of 20 ml.beat^{-1} and 60 beats.min^{-1}. Cardiogenic flow was provided by an oscillating pump connected to the plenum. Turbulence intensity was calculated as the root mean square value of the high-frequency velocity fluctuations obtained.

For carbon dioxide clearance measurements, lung volume changes caused by cardiogenic oscillations were simulated using a flexible diaphragm across the bottom of the plenum that was oscillated by a stepper motor at 60 beats.min^{-1}. The stepper motor was controlled by computer to provide the required cardiogenic flow profiles. Stepper resolution was 0.6 ml.step^{-1}. For each clearance measurement, carbon dioxide was injected into the plenum to achieve an initial concentration of approximately 5%, and THRIVE and cardiogenic oscillations were then started. The carbon dioxide clearance rate was determined from the concentration decay curve time constant.

To determine the required sample size, we obtained measurements that showed carbon dioxide clearance

values measured at 15 ml cardiogenic stroke ranged from mean (SD) 3.8 (0.8) ml.min^{-1} with a THRIVE of 0 l.min^{-1} to 10.5 (1.8) ml.min^{-1} with a THRIVE of 70 l.min^{-1}. At 70 l.min^{-1} THRIVE, clearance values ranged from 1.28 (0.13) ml.min^{-1} with cardiogenic stroke of 0 ml to 55.5 (0.88) ml.min^{-1} with cardiogenic stroke of 40 ml, assuming normal distributions (Shapiro–Wilk normality test: p = 0.77). As such, three measurements at each THRIVE/stroke combination were sufficient to distinguish between clearance values at 60 l.min^{-1} and 70 l.min^{-1} THRIVE and 15 ml stroke (Student's t-test, p < 0.05, power = 80%). We therefore measured clearances at THRIVE flow rates from 0 to 70 l.min^{-1} at 10 l.min^{-1} intervals, with cardiogenic strokes from 0 to 40 ml in 5-ml intervals, taking five measurements at each combination. The THRIVE/stroke combinations were applied in random order. Clearances at different stroke volume/THRIVE flow rate combinations were compared using non-paired, two-tailed Student's t-test. All statistical analyses were performed using Excel (Microsoft, Redmond, USA).

Results

Figure 2 shows flow patterns obtained using particle image velocimetry from the two-dimensional airway model in water with the pharyngeal flow set to be equivalent to a THRIVE of 60 l.min^{-1} in air, and cardiogenic oscillations with an equivalent stroke volume of 9 ml at 60 beats.min^{-1}.

Transnasal humidified rapid-insufflation ventilatory exchange generated a series of strong, linked vortices, extending from the oropharynx to the glottis, which generated substantial turbulence. During cardiogenic inspiration, the lowest vortex was pulled deeper towards the glottis, and turbulence from that vortex was entrained into the trachea, enhancing mixing below the glottis. The entrained turbulence can be seen in Fig. 2a between the trachea and larynx. During cardiogenic expiration, the mixed tracheal fluid was ejected upwards through the glottis and into the vortices just above the larynx (Fig. 2c). The vortices transported it to the flushed region of the oropharynx.

Figure 3 is a series through one cardiogenic cycle of the nebuliser droplet cloud in the trachea from the three-dimensional gas model. The series shows how nebuliser droplets (darker shade = higher droplet density) were transported and cleared from the airway with cardiogenic oscillations applied but no THRIVE (Fig. 3a), and with cardiogenic oscillations plus THRIVE (Fig. 3b). Nebulised droplets were first injected into the carina, and cardiogenic oscillations then started. The sequences show the first
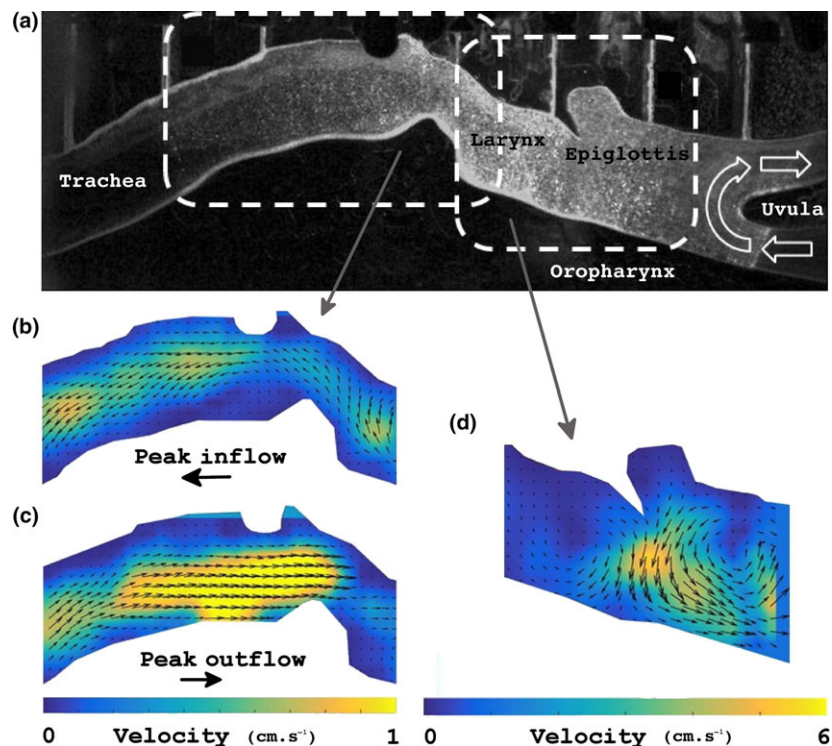
Figure 2 Fluid flow visualisation using particle image velocimetry in a two-dimensional water model of the airway with both high-flow nasal oxygenation and simulated cardiogenic oscillations applied. (a) snapshot of particles in the model; (b) flow vectors at peak cardiogenic inspiration; (c) flow vectors at peak cardiogenic expiration; and (d) flow vectors in the oropharynx.
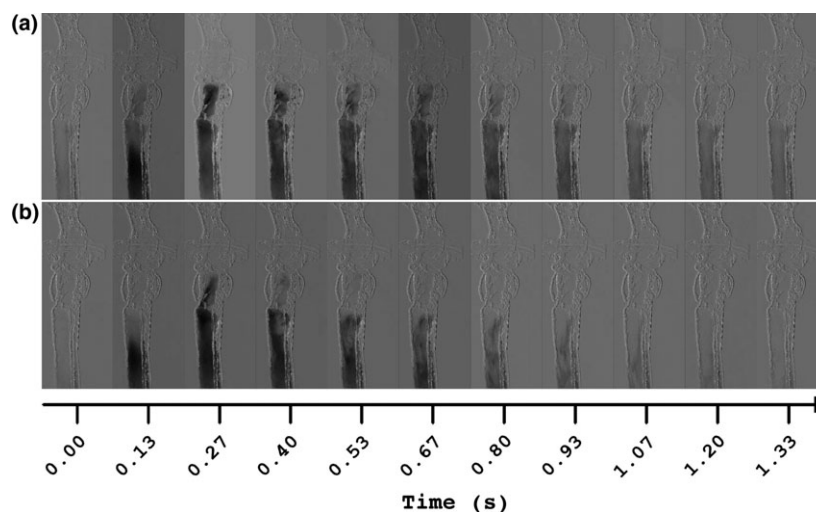
Figure 3 Video frames showing movement and clearance of nebuliser droplets from the trachea of the three-dimensional airway visualisation model over one cardiogenic cycle, with a cardiogenic stroke of 20 ml. (a) Without high-flow nasal oxygen and (b) with high-flow nasal oxygen.

cardiogenic cycle, with initial cardiogenic expiration followed by subsequent cardiogenic inspiration. With no THRIVE applied, the initial cardiogenic expiration brought nebuliser droplets up from the carina to above the glottis. Substantial mixing occurred in the glottis as a result of the inrush of gas from the trachea, but very little nebulised air passed up to the oropharynx. On the subsequent cardiogenic inspiration, almost all the mixed gas was drawn back into the trachea, leaving it filled with low-density droplets from glottis to carina.

The situation was very different when THRIVE was applied. During cardiogenic expiration, the strong vortices existing between the oropharynx and glottis rapidly swept any droplets transported from the trachea up to the oropharynx and out of the mouth, completely flushing the airway from oropharynx to glottis. This can be seen in the image at 0.4 s, at the end of cardiogenic expiration. The result was that during the inspiratory part of the cycle, fresh gas with no residual nebulised droplets was drawn through the glottis and down into the trachea to the carina. At the same time turbulence was entrained into the trachea from the highly turbulent vortices in the pharyngeal region, causing longitudinal intra-tracheal mixing before the next cardiogenic expiration.
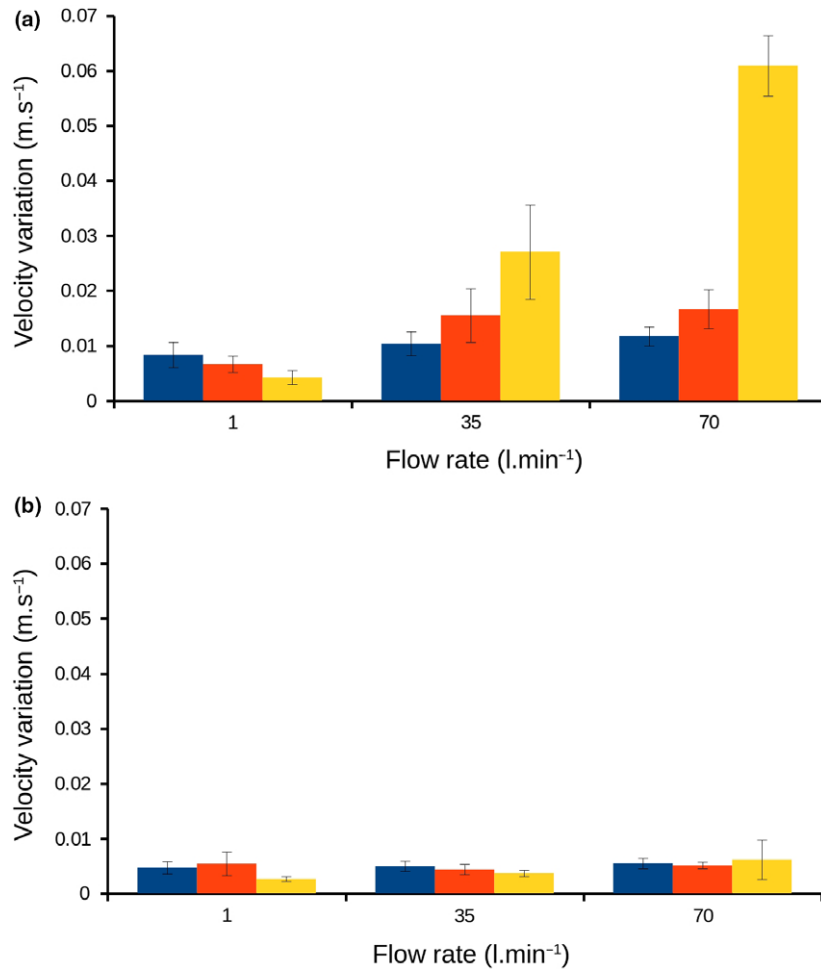
Figure 4 shows turbulence intensity in the three-dimensional gas model at the subglottis, mid-trachea and the lower end of the trachea. We measured the turbulent intensity with a cardiogenic stroke of 20 ml at 60 beats.min^{-1}, separately for the inspiration and expiration phases of the cardiogenic cycle. The bar graphs show the turbulence intensity measured during cardiogenic

inspiration (Fig. 4a) and cardiogenic expiration (Fig. 4b) at each measurement position for THRIVE flow rates of 1 l.min^{-1}, 35 l.min^{-1} and 70 l.min^{-1} averaged over 10 cardiogenic cycles. Turbulence intensity was higher on inspiration than on expiration (p = 0.01 for lower trachea; p = 0.003 for subglottis and mid-trachea). On inspiration, the turbulent intensity increased with THRIVE flow rate, whereas on expiration turbulence intensity appeared unaffected by the flow rate. The turbulence intensity at the bottom of the trachea with THRIVE flow rates of 35 l.min^{-1} and 70 l.min^{-1} at 20 ml stroke was higher on inspiration than expiration, suggesting that entrained turbulence was penetrating the full tracheal length.

Figure 5 shows the variation in carbon dioxide clearance measured in the three-dimensional model as a function of different cardiogenic stroke volumes and THRIVE flow rates. The curves of clearance vs. THRIVE flow rate closely follow functions of the form: Clearance = A + B (1-e$^{-Flow/k}$) at larger cardiogenic strokes, but the value of the parameter k in the fitted curves, which essentially describes how clearance increases with THRIVE flow rate, changes substantially between cardiogenic strokes of 20 ml and 25 ml suggesting changing flow conditions in the trachea.

Discussion

Since Patel and Nouraei reported the use of THRIVE for prolonging the safe apnoea time during shared airway surgery [8], the use of high-flow nasal oxygenation has also been reported for pre-oxygenation [23, 24], awake flexible bronchoscopic intubation [25, 26] and maintenance of saturation during intubation in apnoeic adults [27–29] and

Figure 4 Mean bulk flow turbulence intensity (RMS velocity variation) measured using hot wire anemometry in the three-dimensional airway model at different high-flow nasal oxygen flow rates. (a) during cardiogenic inspiration; and (b) during cardiogenic expiration. Blue = lower trachea; red = mid-trachea; yellow = subglottis. Error bars = 1 SD.
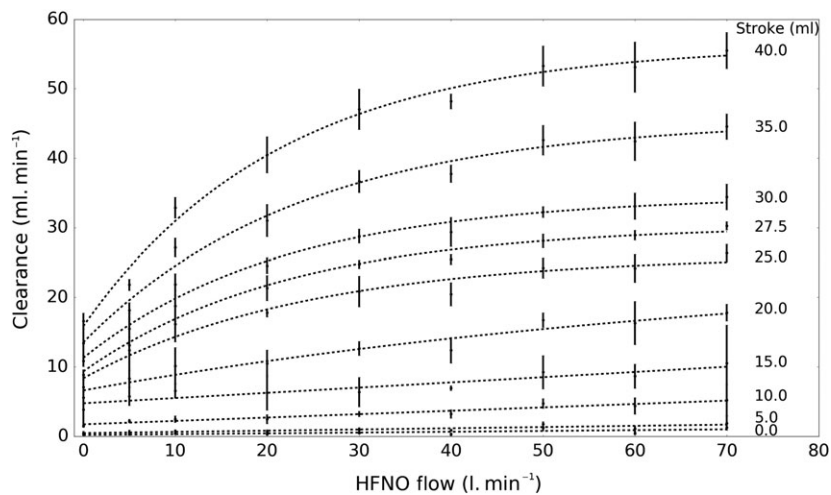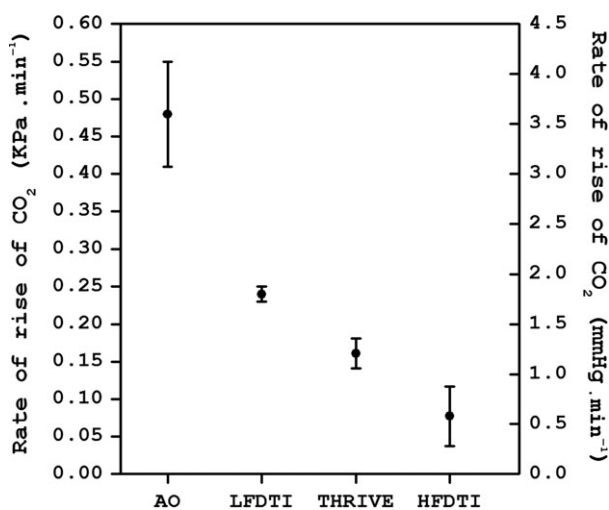

Figure 5 Clearance of carbon dioxide measured in the carbon dioxide clearance experiment. Error bars show ±3 SD at each combination of high-flow nasal oxygen (HFNO)/cardiogenic stroke.

children [30, 31]. Previous work in models [20, 32, 33] and healthy volunteers [34] has described the clearance of carbon dioxide in the upper airway; however, the mechanisms of clearance during apnoea had not been considered.

The average rate of the increase in carbon dioxide during THRIVE, measured by Patel and Nouraei as the slope of the end of procedure ET_{CO2} against time, was 0.15 kPa.min^{-1} [8]. Gustafsson et al. found the average rate of increase in $PaCO_2$, measured using arterial blood gas sampling, to be 0.24 kPa.min^{-1} [12]. These values for the rate of increase in carbon dioxide fall between values observed when direct intra-tracheal oxygen insufflation between 0.5 l.min^{-1} and 45 l.min^{-1} was used (Fig. 6) [35, 36]. Other workers have also published results indicating that the rate of increase in carbon dioxide with THRIVE is lower than in classical apnoeic oxygenation [13, 14].

Our work indicates that an interaction of gas flow from cardiogenic oscillations and high-flow nasal oxygenation provides a mechanism for transporting carbon dioxide from the carina to the pharynx. We would expect an improvement in oxygen transport to go hand-in-hand with the enhancement of carbon dioxide clearance. Together with the airway pressure generated by the high flow that reduces atelectasis [37, 38], this explains, in part, the

dramatic increases in time before desaturation observed with THRIVE [8, 12] compared with lower nasal flow rates.

The volume of the adult trachea is typically between 25 ml and 35 ml [39], whereas the literature indicates that the volume of cardiogenic oscillations is typically 6–40 ml [19, 40–42]. Taylor dispersion causes longitudinal spreading of a plug gas flowing in a pipe [43], and this will mix gas longitudinally in the trachea in analogous fashion to the longitudinal mixing demonstrated by van der Kooij and Luijendijk in the bronchi [44]. This accounts for some of the carbon dioxide clearance observed clinically, and suggests that even in classical apnoeic oxygenation with no high flow, there could be a small amount of carbon dioxide clearance as seen in Fig. 5.

Our experiments indicate that Taylor dispersion is not the only mechanism causing mixing of gas in the trachea. Our visualisation of flow showed turbulent eddies in the pharynx caused by THRIVE being entrained into the trachea during cardiogenic inspiration. This was confirmed by hot wire anemometry, which showed higher levels of turbulence during cardiogenic inspiration than during cardiogenic expiration. The levels of turbulence were related to the THRIVE flow rate.

Our experiments have several limitations. Our models only investigated clearance from the carina to the atmosphere. They were not intended to accurately measure clearance from the lung periphery. However, there is already good evidence that mixing occurs between the alveoli and the bronchi or lower trachea through cardiogenic oscillations [15, 16]. Although there is likely to be a carbon dioxide gradient between the lung periphery and the carina, our experiments indicate that the combined influence of cardiogenic oscillations and THRIVE is able to transport carbon dioxide from carina to mouth.

A further limitation is that our models were not compliant but printed from hard plastic. The gross pressure variations caused by turbulence in the pharynx are therefore likely to cause less random bulk inflow and outflow into the glottis and trachea, and this may also give rise to less clearance than may be clinically observed. Our models were also not able to model cardiogenic pulsations of the trachealis muscle that are commonly seen during endoscopy [45]. This will cause additional mixing within the trachea, further enhancing clearance rate.

The carbon dioxide clearance rates that we measured were substantially less than the rate of production for a resting adult of approximately 200 ml.min^{-1}. Even though the clearance rate will increase with increasing carbon dioxide concentration in the lungs, this will still be lower than the rate of production, and consequently arterial

Figure 6 Comparison of the rates of rise of carbon dioxide under different oxygenation conditions. AO, apnoeic oxygenation/airway obstruction, combined data mean (95%CI) [11, 46–48]; LFDTI, low-flow direct tracheal insufflation with intra-tracheal catheter at a rate of 0.5 l.min^{-1} [35]; THRIVE, transnasal humidified rapid-insufflation ventilatory exchange, slope (95%CI) [8]. HFDTI: high-flow direct tracheal insufflation via tracheal tube at 45 l.min^{-1}, mean (95%CI) [36].

carbon dioxide will accumulate during high-flow nasal oxygenation. Workers such as Fraioli et al. [46] and Stock et al. [47] have demonstrated buffering of carbon dioxide in the blood in apnoea, and Gustafsson et al. [12] have shown this also occurs in THRIVE. Clinical evidence indicates that even the small additional clearance of carbon dioxide in THRIVE reduces the buffering load, increasing the time until carbon dioxide retention becomes problematic.

Our work shows that high-flow nasal oxygenation, operating in conjunction with cardiogenic oscillations, enhances the clearance of carbon dioxide in apnoea, thus explaining apnoeic gas exchange. We have shown by flow visualisation, measurement of flow turbulence and carbon dioxide elimination in two-dimensional liquid and three-dimensional gas models, the influence of high-flow nasal oxygenation and cardiogenic oscillations on flow vortices, tracheal extension, flow turbulence and carbon dioxide clearance. Carbon dioxide clearance during THRIVE is mediated by the interaction between supraglottic flow vortices and flow oscillations caused by cardiogenic oscillations.

Acknowledgements

References

1. Hernández G, Roca O, Colinas L. High-flow nasal cannula support therapy: new insights and improving performance. *Critical Care* 2017; **21**: 62.
2. Nishimura M. High-flow nasal cannula oxygen therapy in adults: physiological benefits, indication, clinical benefits, and adverse effects. *Respiratory Care* 2016; **61**: 529–41.
3. Ischaki E, Pantazopoulos I, Zakynthinos S. Nasal high flow therapy: a novel treatment rather than a more expensive oxygen device. *European Respiratory Reviews* 2017; **26**: 170028.
4. Mikalsen IB, Davis P, Øymar K. High flow nasal cannula in children: a literature review. *Scandinavian Journal of Trauma Resuscitation and Emergency Medicine* 2016; **24**: 93.
5. Vincent J-L. High-flow oxygen cannula: a very effective method to correct severe hypoxemia. *Journal of Thoracic Disease* 2015; **7**: E207–8.
6. Hernández G, Vaquero C, González P, et al. Effect of postextubation high-flow nasal cannula vs conventional oxygen therapy on reintubation in low-risk patients: a randomized clinical trial. *Journal of the American Medical Association* 2016; **315**: 1354–61.
7. Frat J-P, Thille AW, Mercat A, et al. High-flow oxygen through nasal cannula in acute hypoxemic respiratory failure. *New England Journal of Medicine* 2015; **372**: 2185–96.
8. Patel A, Nouraei SA. Transnasal humidified rapid-insufflation ventilatory exchange (THRIVE): a physiological method of increasing apnoea time in patients with difficult airways. *Anaesthesia* 2015; **70**: 323–9.
9. Draper WB, Whitehead RW, Spencer JN. Studies on diffusion respiration. III. Alveolar gases and venous blood pH of dogs during diffusion respiration. *Anesthesiology* 1947; **8**: 524–33.
10. Bartlett RG Jr, Brubach HF, Specht H. Demonstration of aventilatory mass flow during ventilation and apnea in man. *Journal of Applied Physiology* 1959; **14**: 97–101.
11. Frumin MJ, Epstein RM, Cohen G. Apneic oxygenation in man. *Anesthesiology* 1959; **20**: 789–98.
12. Gustafsson I-M, Lodenius Å, Tunelli J, Ullman J, Jonsson Fagerlund M. Apnoeic oxygenation in adults under general anaesthesia using transnasal humidified rapid-insufflation ventilatory exchange (THRIVE) – a physiological study. *British Journal of Anaesthesia* 2017; **118**: 610–17.
13. Hengen M, Bischoff G, Koessler S, et al. Changes in transcutaneous carbon dioxide tension during apneic oxygenation for suspension laryngoscopy. ASA Abstracts 2017: A1265. http://www.asaabstracts.com/strands/asaabstracts/ abstract.htm?year=2017&index=19&absnum=5135 (accessed 11/12/2018).
14. To K, Harding F, Scott M, et al. The use of transnasal humidified rapid-insufflation ventilatory exchange in 17 cases of subglottic stenosis. *Clinical Otolaryngology* 2017; **42**: 1407–10.
15. Slutsky AS. Gas mixing by cardiogenic oscillations: a theoretical quantitative analysis. *Journal of Applied Physiology Respiratory Environmental and Exercise Physiology* 1981; **51**: 1287–93.
16. Slutsky AS, Brown R. Cardiogenic oscillations: a potential mechanism enhancing oxygenation during apneic respiration. *Medical Hypotheses* 1982; **8**: 393–400.
17. Haycraft JB, Edie R. The cardiopneumatic movements. *Journal of Physiology* 1891; **12**: 426–37.
18. Arieli R. Cardiogenic oscillations in expired gas: origin and mechanism. *Respiration Physiology* 1983; **52**: 191–204.
19. Tusman G, Suarez-Sipmann F, Peces-Barba G, et al. Pulmonary blood flow generates cardiogenic oscillations. *Respiratory Physiology and Neurobiology* 2009; **167**: 247–54.
20. Van Hove SC, Storey J, Adams C, et al. An experimental and numerical investigation of CO_2 distribution in the upper airways during nasal high flow therapy. *Annals of Biomedical Engineering* 2016; **44**: 3007–19.
21. Womersley JR. Method for the calculation of velocity, rate of flow and viscous drag in arteries when the pressure gradient is known. *Journal of Physiology* 1955; **127**: 553–63.
22. Lee JS. The mixing and axial transport of smoke in oscillatory tube flows. *Annals of Biomedical Engineering* 1984; **12**: 371–83.
23. Frerk C, Mitchell VS, McNarry AF, et al. Difficult Airway Society 2015 guidelines for management of unanticipated difficult intubation in adults. *British Journal of Anaesthesia* 2015; **115**: 827–48.
24. Mushambi MC, Kinsella SM, Popat M, et al. Obstetric Anaesthetists' Association and Difficult Airway Society guidelines for the management of difficult and failed tracheal intubation in obstetrics. *Anaesthesia* 2015; **70**: 1286–306.
25. Badiger S, John M, Fearnley RA, Ahmad I. Optimizing oxygenation and intubation conditions during awake fibre-optic intubation using a high-flow nasal oxygen-delivery system. *British Journal of Anaesthesia* 2015; **115**: 629–32.
26. El-Boghdadly K, Onwochei DN, Cuddihy J, Ahmad I. A prospective cohort study of awake fibreoptic intubation practice at a tertiary centre. *Anaesthesia* 2017; **72**: 694–703.
27. Mir F, Patel A, Iqbal R, Cecconi M, Nouraei SAR. A randomised controlled trial comparing transnasal humidified rapid insufflation ventilatory exchange (THRIVE) pre-oxygenation with facemask pre-oxygenation in patients undergoing rapid sequence induction of anaesthesia. *Anaesthesia* 2017; **72**: 439–43.

28. Lodenius Å, Piehl J, Östlund A, Ullman J, Jonsson Fagerlund M. Transnasal humidified rapid-insufflation ventilatory exchange (THRIVE) vs. facemask breathing pre-oxygenation for rapid sequence induction in adults: a prospective randomised non-blinded clinical trial. *Anaesthesia* 2018; **73**: 564–71.

29. Nekhendzy V. Lights! Oxygen! Action! Hollywood anaesthesia is coming to a theatre near you. *British Journal of Anaesthesia* 2017; **118**: 489–91.

30. Humphreys S, Lee-Archer P, Reyne G, Long D, Williams T, Schibler A. Transnasal humidified rapid-insufflation ventilatory exchange (THRIVE) in children: a randomized controlled trial. *British Journal of Anaesthesia* 2017; **118**: 232–8.

31. Jagannathan N, Burjek N. Transnasal humidified rapid-insufflation ventilatory exchange (THRIVE) in children: a step forward in apnoeic oxygenation, paradigm-shift in ventilation, or both? *British Journal of Anaesthesia* 2017; **118**: 150–2.

32. Spence CJT, Buchmann NA, Jermy MC, Moore SM. Stereoscopic PIV measurements of flow in the nasal cavity with high flow therapy. *Experiments in Fluids* 2010; **50**: 1005–17.

33. Möller W, Celik G, Feng S, et al. Nasal high flow clears anatomical dead space in upper airway models. *Journal of Applied Physiology* 1985; **2015**: 1525–32.

34. Möller W, Feng S, Domanski U, et al. Nasal high flow reduces dead space. *Journal of Applied Physiology* 1985; **2017**: 191–7.

35. Rudlof B, Hohenhorst W. Use of apneic oxygenation for the performance of pan-endoscopy. *Otolaryngology - Head and Neck Surgery* 2013; **149**: 235–9.

36. Watson RJ, Szarko R, Mackenzie CF, Sequeira AJ, Barnas GM. Continuous endobronchial insufflation during internal mammary artery harvest. *Anesthesia and Analgesia* 1992; **75**: 219–25.

37. Ritchie JE, Williams AB, Gerard C, Hockey H. Evaluation of a humidified nasal high-flow oxygen system, using oxygraphy, capnography and measurement of upper airway pressures. *Anaesthesia and Intensive Care* 2011; **39**: 1103–10.

38. Parke R, McGuinness S, Eccleston M. Nasal high-flow therapy delivers low level positive airway pressure. *British Journal of Anaesthesia* 2009; **103**: 886–90.

39. Kamel KS, Lau G, Stringer MD. In vivo and in vitro morphometry of the human trachea. *Clinical Anatomy* 2009; **22**: 571–9.

40. Colebatch HJH, Ng CKY, Maccioni FJ. Inspiratory gas flow induced by cardiac systole. *Respiration Physiology* 1996; **105**: 103–8.

41. Montmerle S, Linnarsson D. Effects of gravity and blood volume shifts on cardiogenic oscillations in respired gas. *Journal of Applied Physiology* 1985; **2005**: 931–6.

42. Collier GJ, Marshall H, Rao M, Stewart NJ, Capener D, Wild JM. Observation of cardiogenic flow oscillations in healthy subjects with hyperpolarized ^{3}He MRI. *Journal of Applied Physiology* 1985; **2015**: 1007–14.

43. Aris R. On the dispersion of a solute in pulsating flow through a tube. *Proceedings of the Royal Society of London. Series A. Mathematical and Physical Sciences* 1960; **259**: 370–6.

44. van der Kooij AM, Luijendijk SC. Longitudinal dispersion of gases measured in a model of the bronchial airways. *Journal of Applied Physiology* 1985; **59**: 1343–9.

45. Nouraei SA. Normal trachea, 2007. https://www.youtube.com/watch?v=VQnfRc3ODgs. (accessed 15/11/2018).

46. Fraioli RL, Sheffer LA, Steffenson JL. Pulmonary and cardiovascular effects of apneic oxygenation in man. *Anesthesiology* 1973; **39**: 588–96.

47. Stock MC, Schisler JQ, McSweeney TD. The PaCO$_2$ rate of rise in anesthetized patients with airway obstruction. *Journal of Clinical Anesthesia* 1989; **1**: 328–32.

48. Eger EI, Severinghaus JW. The rate of rise of Pa$_{CO2}$ in the apneic anesthetized patient. *Anesthesiology* 1961; **22**: 419–25.